

# Connecting Pixels to Privacy and Utility: Automatic Redaction of Private Information in Images

Tribhuvanesh Orekondy    Mario Fritz    Bernt Schiele

Max Planck Institute for Informatics  
Saarland Informatics Campus  
Saarbrücken, Germany

{orekondy,mfritz,schiele}@mpi-inf.mpg.de

## Abstract

Images convey a broad spectrum of personal information. If such images are shared on social media platforms, this personal information is leaked which conflicts with the privacy of depicted persons. Therefore, we aim for automated approaches to redact such private information and thereby protect privacy of the individual.

By conducting a user study we find that obfuscating the image regions related to the private information leads to privacy while retaining utility of the images. Moreover, by varying the size of the regions different privacy-utility trade-offs can be achieved. Our findings argue for a “redaction by segmentation” paradigm.

Hence, we propose the first sizable dataset of private images “in the wild” annotated with pixel and instance level labels across a broad range of privacy classes. We present the first model for automatic redaction of diverse private information. It is effective at achieving various privacy-utility trade-offs within 83% of the performance of redactions based on ground-truth annotation.

## 1. Introduction

More and more visual data is captured and shared on the Internet. Images and video contain a wide range of private information that may be shared unintentionally such as e.g. email-address, picture-id or finger-print (see Figure 1). Consequently, there is a growing interest within the computer vision community [4, 16, 20, 22, 38, 40] to assess the amount of leaked information, understand implications on privacy and ultimately control and enforce privacy again. Yet, we are missing an understanding how image content relates to private information and how automated redaction can be approached.

Therefore, we address two important questions in this

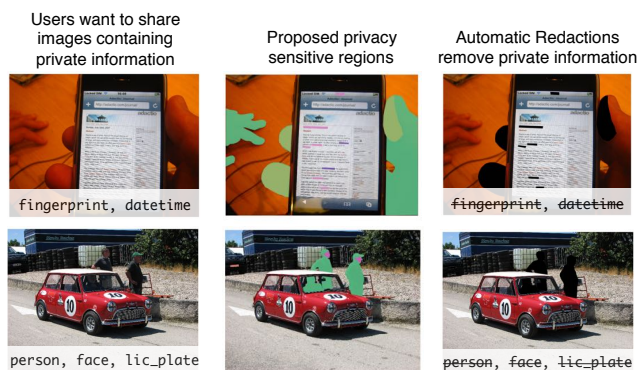


Figure 1: Users often share images containing private information on the Internet, which poses a privacy risk. For example, in the top row, user might unintentionally leak their fingerprint. We present methods to aid users automatically redact such content by proposing privacy sensitive regions in images.

context. First, how can private information be redacted while maintaining an intelligible image? We investigate this question in a user study with highly encouraging results: we can redact private information in images while preserving its utility. Furthermore, varying the amount of pixels redacted results in different privacy vs. utility trade-offs. We conclude that redaction by segmentation is a valid approach to perform visual redactions.

We ask a second question in this paper: What kind of privacy-utility trade-offs can be achieved by automatic redaction schemes? Based on our first finding, we approach this as a pixel labeling task on multiple privacy classes (which we refer to as *privacy attributes*). Segmenting privacy attributes in images presents a new challenge of reasoning about regions including multiple modalities. For instance, in Figure 1, identifying the name and date-time re-

quires mapping the relevant pixels to the text domain for understanding, while identifying the `student_id` requires reasoning over both visual and text domains. Our automated methods address these challenges and localize these privacy attributes for redaction via segmentation. By performing both quantitative and human evaluation, we find these automated methods to be effective in segmentation as well as privacy-utility metrics.

Our model and evaluation for automatic redaction is facilitated by a new dataset that extends the Visual Privacy (VISPR) dataset [38] to include high-quality pixel and instance-level annotations. To this end, we propose a dataset containing 8.5k images annotated with 47.6k instances over 24 privacy attributes. We will make the dataset publicly available for future research.

## 2. Related Work

**Text Sanitation** Redaction techniques are primarily studied in the context of confidential text documents, wherein certain sensitive entities need to be removed. Studies focus on identification of such entities [5, 8, 9, 41, 42, 43] and methods to prevent over-sanitation [5, 41]. However, unlike these works which have access to dense structured text data (e.g. documents), we deal with unstructured pixel-level representations of such entities.

**Image Perturbations for Privacy** Adversarial perturbations [15, 18, 36] are suggested to evade person identification [22, 45]. However, these methods typically assume a white-box CNN-based adversary for the specific task of face recognition. In contrast, we propose redacting content at the expense of some utility to achieve better privacy (measured against humans) across a broad range of privacy classes. [4] proposes de-identifying people by generating an alternate appearance for the person. We study a more fundamental problem of identifying such regions where such methods could be directly applicable. [27, 29] study obfuscation of private content, but are limited to constrained surveillance videos and non-automated methods.

**Private Information Recognition** Many existing studies focus on either detecting faces [47, 49], license plates [6, 53, 54], relationships [46, 50], age [3] or occupations [44]. Research in determining privacy risk across a broad range of privacy classes are typically treated as a classification problem [38, 48, 51]. However, many studies [2, 11] demonstrate a “privacy paradox” – users share such images in spite of knowing the privacy risks. Hence in this work, we propose a middle ground for reducing privacy leakage, such that users can still share images by redacting private content while preserving its utility.

**Visual Privacy Datasets** PicAlert [52] and YourAlert [51] propose datasets with user-classified privacy labels. VISPR [38] provides a more exhaustive dataset of 22k im-

ages annotated with a broad range of image-level privacy labels. The PEViD video dataset [28] provides person-centric bounding box annotation over 20 video sequences in a constrained setting. In contrast, our dataset based on VISPR images provides pixel level annotation from a diverse set of privacy classes.

**Segmentation** Identifying pixel-level labels from images is a well-studied problem in computer vision. However, most methods [32, 34] and datasets [10, 13, 33] focus on segmenting common objects in visual scenes. We however focus on identifying private regions in a privacy-utility framework, which introduces many new challenges.

## 3. The Visual Redactions Dataset

In this section we present our pixel-label visual privacy dataset as an extension to the VISPR dataset [38]. We begin with a discussion on how images (Section 3.1) and attributes (Section 3.2) were selected for the task. This is followed by the annotation procedure (Section 3.3) and a brief analysis (Section 3.4) of the dataset.

### 3.1. Selecting Images for Pixel-level Annotation

The VISPR dataset contains 22k real-world user-uploaded publicly available Flickr images which makes this a great starting point for addressing the visual redaction problem “in the wild”. 10k of these images are annotated as safe. From the remaining 12k images we pixel-annotate the subset of 8,473 images that contain at most 5 people. The main reason to focus on this subset was to reduce the annotation cost while maximizing the amount of non-person pixels. We preserve the identical 45-20-35 train-val-test split of these images as in the VISPR dataset.

### 3.2. Shortlisting Privacy Attributes

The 22k images in the multilabel VISPR dataset are annotated using 68 image-level privacy attributes ( $\sim 5.2$  attributes per image). These privacy attributes are compiled from multiple privacy-relevant sources – the US Privacy Act of 1974, EU Data Protection Directive 95/46/EC and various social network website rules. Additionally, they cover a diverse range of private information that can be leaked in images (e.g. face, tattoo, physical disability, personal relationships, passport, occupation). Therefore, we use these as a starting point for redactions in images. We select 42 out of 67 privacy attributes (excluding attribute safe) for three reasons. First, for 11 attributes (e.g. religion, occupation, sports) typically the entire image is linked to the attribute (e.g. scene with church or sport stadium). In such cases, the solution to keeping the information private is to not share such images (as proposed in [38]). We instead focus on attributes which can be localized for redaction, such that the image might still be useful. Second, 8 attributes were

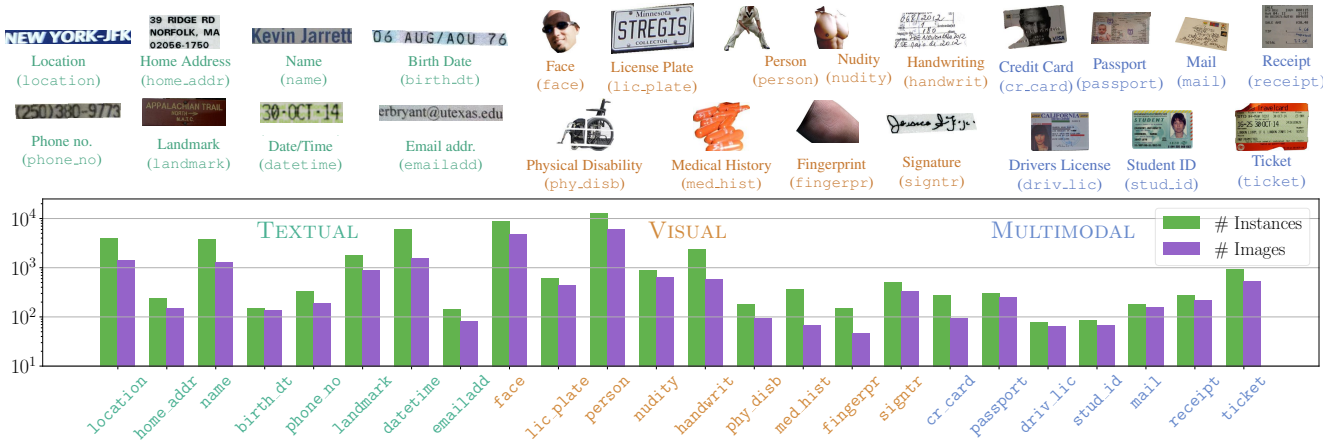


Figure 2: Examples and distribution of privacy attributes in the dataset.

extremely tedious to annotate, because of their strong co-occurrence with crowd-scenes (e.g. political and general opinion, occupation) or the effort required to outline them (e.g. hair color). Third, 6 attributes (e.g. place of birth, email content, national id) contained under 30 examples for training. In spite of filtering such attributes, we still cover a broad spectrum of information to help de-identify people in images (such as by obfuscating faces or names). We further merge few groups among these 42 attributes: (i) when they occur as a complete and partial version (e.g. (complete face, partial face) merged into face) (ii) when they localize to the same region (e.g. (race, skin color, gender, relationships) merged into person). As a result, we work with 24 localizable privacy attributes in our dataset representative of 42 of the original 67 VISPR privacy attributes (see Figure 2 for the complete list).

### 3.3. Dataset Annotation

In this section, we discuss the annotation procedure.

**Annotation Tool and Instructions** We use a customized version of the VGG Image Annotator tool [12]. Five expert annotators draw polygons around instances based on an instruction manual. A summary of instructions, definitions of attributes and examples are provided in the supplementary material.

**Consensus and Agreement Measure** Agreement is calculated w.r.t. images annotated by one of the authors. We measure agreement using Mean Intersection Over Union (mIoU):  $\sum \frac{tp}{tp+fp+fn}$  averaged over images.

**Consensus Experiment and Annotating person** We observed 93.8% agreement in consensus task of annotating instances of person in 272 images. Annotators separately annotated person in remaining images. With an annotation effort of  $\sim 240$  hours, we obtain 13,171 person instances annotated over 5,920 images.

**Annotating face** We observed an agreement of 86.2% (lower due to small sizes of instances) in the consensus task for annotating face in 100 images. Using the 5,920 images of people as a starting point, annotators annotated faces in separate sets of images. In  $\sim 60$  hours, we gather 8,996 instances of faces.

**Annotating Remaining Attributes** Images for each of the remaining 22 attributes are annotated together successively by at most a single annotator. 8 of the text-based attributes (e.g. name, phone\_no) are annotated using 4-sided polygons or bounding boxes. Over  $\sim 220$  hours, we gather annotation of 26,676 instances.

**Text Annotations** We augment all images in the dataset with text detections obtained using the Google Cloud Vision API to aid localization of text-based attributes. This is provided as OCR and bounding box annotation in structured hierarchy of text elements in the order: characters, words, paragraphs, blocks and pages. In addition, we also gather face and landmark bounding box detections using the same API.

**Summary** With an annotation effort of  $\sim 800$  hours concentrated over four months with five annotators (excluding the authors), we propose the first sizable pixel-labeled privacy dataset of 8,473 images annotated with  $\sim 47.6k$  instances using 24 privacy attributes.

### 3.4. Dataset Analysis and Challenges

We now present a brief analysis of the dataset and the new challenges it presents for segmentation tasks. Examples of the proposed attributes and their distribution among the 8k images in the dataset are presented in Figure 2.

Popular datasets [10, 13, 33] provide pixel-level annotation of various common visual objects. These objects are common in visual scenes, such as vehicles (car, bicycle), animals (dog, sheep) or household items (chair, table). Common to all these objects are their distinctive visual cues.



Figure 3: Dilation/Erosion of attribute fingerprint

Looking at the examples of attributes in Figure 2, one can notice similar cues among the VISUAL attributes, but it is not evident in the others. Recognizing TEXTUAL attributes (such as names or phone numbers) in images instead require detecting and parsing text information and additionally associating it with prior knowledge. While some of the MULTIMODAL attributes can be associated with visual cues, often the text content greatly helps disambiguate instances (a card-like object could be a `student_id` or `driv_lic`). We also observe a strong correlation between modalities and sizes of instances. We find TEXTUAL instances to occupy on average less than 1% of pixels in images, while the MULTIMODAL attributes predominantly occur as close-up photographs occupying 45% of the image area on average. Consequently, the privacy attributes pose challenges from multiple modalities and require specialized methods to individually address them. Moreover, they provide different insights due to the variance in sizes. Hence, going forward, we treat the modes TEXTUAL, VISUAL and MULTIMODAL as categories to aid analysis and addressing challenges presented by them.

**Applicability to other problems** We believe the proposed dataset could be beneficial to many other problems apart from visual redactions. In visual privacy, it complements datasets to perform tasks such as person de-identification [4, 16]. Outside of the privacy domain, we also provide a sizable face segmentation dataset with 9k face instances, compared to 2.9k in Labeled Faces in the Wild [23] and 200 in FASSEG [24].

## 4. Understanding Privacy and Utility w.r.t. Redacted Pixels

In this section, we study how redacting ground-truth pixels of attributes influences privacy and utility of the image by conducting a user study on Amazon Mechanical Turk (AMT). We will also use the results from this study as a reference point for evaluating our proposed automated methods in Section 6.2.

### 4.1. Generating Redactions

Given an image  $I_a$  containing attribute  $a$ , we generate a ground-truth redacted version of the image  $I_{\bar{a}}$  by simply blacking-out pixels corresponding to  $a$  in the ground-truth.

**Spatially extending  $a$**  We now want to redact fewer or more pixels in image  $I_{\bar{a}}$  to understand how this influences the image’s privacy and utility. We generate multiple

versions of the ground-truth redacted image  $\{I_{\bar{a}}^s : s \in S\}$  at different scales of redaction, such that  $I_{\bar{a}}^{n,s}$  contains  $n$  times as many blacked-out pixels of  $I_{\bar{a}}^s$ . We achieve different scales of redactions by dilating/eroding the ground-truth binary mask of  $a$ , as shown in Figure 3. We use seven scales  $S = \{0.0, 0.25, 0.5, 1.0, 2.0, 4.0, \text{inf}\}$ , where  $I_{\bar{a}}^0$  is the unredacted image,  $I_{\bar{a}}^1 (= I_{\bar{a}})$  is the GT redacted image and  $I_{\bar{a}}^{\text{inf}}$  is a completely blacked-out image.

### 4.2. User Study

We create an AMT project of 1,008 tasks (24 attributes  $\times$  6 images  $\times$  7 scales), each to be responded by 5 unique workers from a pool of 29 qualified workers. Each task contains 2 yes/no questions based on an image  $I_{\bar{a}}^s$ , one each for Privacy and Utility. We consider *privacy* and *utility* w.r.t. (i) two versions of the same image:  $(I_a, I_{\bar{a}}^s)$ , and (ii) users (AMT workers in our case).

**Defining Privacy** To understand if attribute  $a$  has been successfully redacted in  $I_{\bar{a}}^s$ , we pose the privacy question in the form: “Is  $a$  visible in the image?”. We also provide a brief description of the attribute  $a$  along with examples. We consider  $I_{\bar{a}}^s$  to be *private*, if a majority of the users respond *no*.

**Defining Utility** To understand utility of an image, we pose the question: “Is the image intelligible, so that it can be shared on social networking websites? *i.e.* does this image convey the main content of the original image (*i.e.*, the image without the black patch)”. As a result, we define the utility of an image independent to its aesthetic value and instead associate it with the semantic information. We consider  $I_{\bar{a}}^s$  to have *utility*, if a majority of the users respond *yes*.

**Measuring Privacy and Utility** We label each of the 1,008 images with varying redacted scales their privacy and utility as discussed above. For any given redaction scale  $s$ , we aggregate privacy/utility scores simply as the percentage of images considered private/useful. Consequently, an ideal visual redaction has both high privacy and utility.

### 4.3. Analysis

We now discuss results based on the privacy-utility scores obtained over modes and various sizes (*i.e.* relative size of  $a$  in  $I_a$ ) based on Figure 4.

**Privacy is a Step Function** We observe in Figure 4 across all plots, that a minimum number of pixels of attribute  $a$  need to be removed to effectively redact it from the image. This minimum number corresponds to exactly the ground-truth redaction ( $s = 1$ ) – redacting fewer pixels than this makes the image non-private and redacting more pixels achieves marginal privacy gains. More specifically, we achieve 94% privacy with ground-truth redactions. The imperfect privacy score is predominantly (5/9 failure cases)

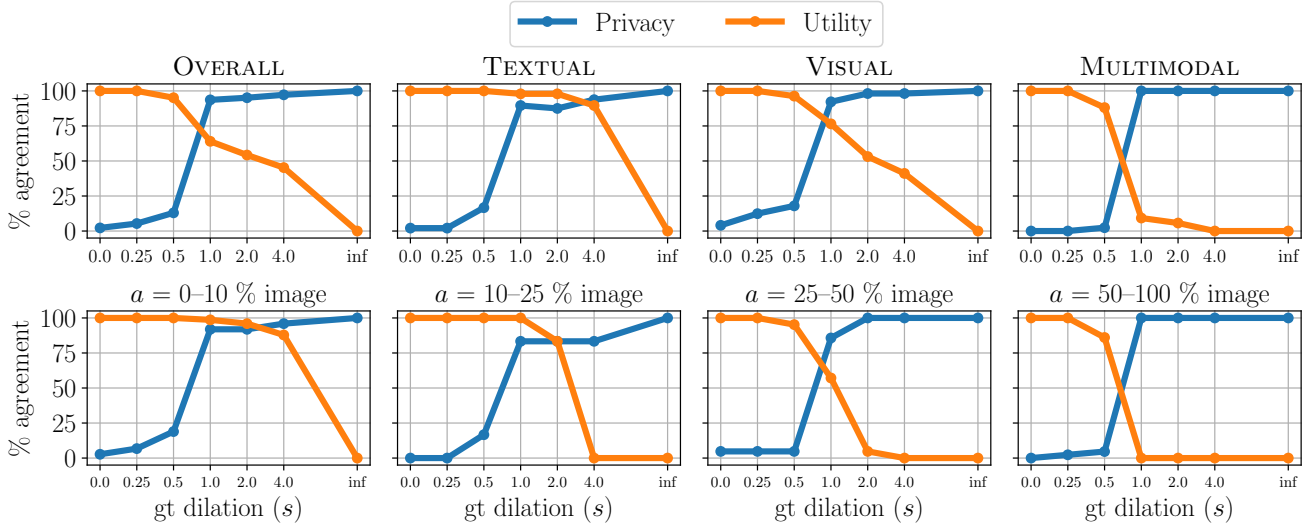


Figure 4: Privacy and Utility using various scales of ground-truth redaction over (Top row) modes (Bottom row) sizes

due to turkers overlooking important details in the question. Apart from this, other cases involve contextual cues revealing the attribute (e.g. shadow of a wheelchair) and regions that were not annotated (e.g. outline of a person at a distance).

**Gradual Loss in Utility** From Figure 4 OVERALL, we find utility to decrease gradually as the size of redacted region increases. Another interesting observation is that utility strongly depends on the size of  $a$  in the image. In the bottom row of Figure 4, we see that for smaller GT regions ( $a = 0 - 10\%$ ), we still obtain high utility at larger dilations. However, as the area of the GT regions increases beyond 50% of the image, redaction entails blacking-out the majority of the image pixels and hence zero utility.

**Privacy and Utility** What can we take away from this while proposing automated methods to preserve privacy while retaining utility? Due to the correlation between modes and sizes, we can predict more pixels for smaller attributes with minimal loss to utility. For instance, for TEXTUAL attributes, we can predict 4x as many ground-truth pixels for redaction. However, for larger ground-truth regions ( $>50\%$  of image) both privacy and utility are step functions and hence making redaction a choice between privacy and utility.

**GT Segmentations are a Good Proxy** In general, for images over all attributes and sizes (Figure 4 OVERALL), we see that we can already achieve high privacy *while* retaining considerable utility of the image. Moreover, we obtain near-perfect privacy with the highest utility in all cases at  $s = 1$ , the ground-truth redactions. This justifies to address privacy attribute redaction as a segmentation task.

## 5. Pixel-Labeling of Private Regions

In Section 3 we discussed the challenges of attributes occurring across multiple modalities (TEXTUAL, VISUAL, MULTIMODAL). In Section 4, we motivated how ground-truth segmentations in our dataset make a good proxy for visual redactions. In this section we propose automated methods to perform pixel-level labeling (semantic segmentation) of privacy attributes in images, with an emphasis on methods tackling each modality.

We begin with a simple baseline **Nearest Neighbor (NN)**: A 2048-dim feature is extracted using ResNet-50 for each image. At test time, we predict the segmentation mask of the closest training image in terms of  $L_2$  distance.

### 5.1. Methods for TEXTUAL-centric attributes

To facilitate segmenting textual attributes, for each image we first obtain an ordered sequence of bounding box detections of words and their OCR using the Google Cloud Vision API (as discussed in Section 3.3).

**Proxy GT** We represent  $n$  words in an image as a sequence  $[(w_i, b_i, y_i)]_{i=1}^n$ , where  $w_i$  is the word text,  $b_i$  is the bounding box and  $y_i$  is the label. We use 9 labels (8 TEXTUAL attributes + safe). We assign each  $y_i$  in the sequence the ground-truth attribute that maximally overlaps with  $b_i$ , or a *safe* label in case of zero overlap. At test-time, we segment pixels in region  $b_i$  if a non-safe label is predicted for word  $w_i$ . For the test set, we refer to predictions from this proxy dataset as **PROXY** to obtain an upper-bound for our methods on these text detections.

**Rule-based Classification (RULES)** We use the following rules to label words in the sequence: (i) *name*: if it exists in a set of 241k names obtained from the US Census Bureau website. (ii) *location*, *landmark*, *home\_address*: if it

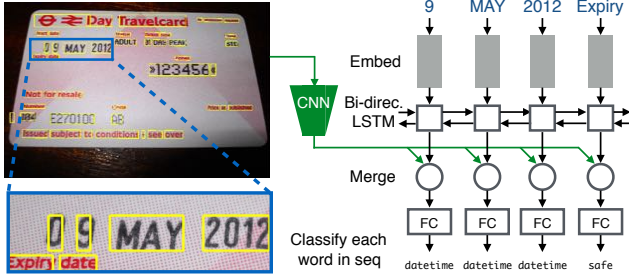


Figure 5: Architecture to perform Sequence Labeling

exists in a set of 3.7k names of cities and countries from Wikipedia’s list of locations with a population of more than 110k. (iii) `datetime`, `phone_no`, `birth_dt`: if the word contains a digit (iv) `emailadd`: if the word contains the symbol @, we predict this word and adjacent words assuming a format `□@□.□`

**Named Entity Recognition (NER)** We use the popular Stanford NER CRFClassifier [14] to label each word of the sequence as from a set of recognized entity classes (e.g. person, organization, *etc.*). We use the model which is trained on case-invariant text to predict one of seven entity classes.

**Sequence Labeling (SEQ)** We train a sequence labeler similar to [19, 31, 35] as shown in Figure 5. We preprocess by replacing all digits with 0s and stem each word to reduce the size of the vocabulary. We tokenize the words in the training sequences using a vocabulary of size 4,149 (number of words with at least 4 occurrences). We embed the words using 100-d GloVe embeddings [39]. To capture the temporal nature, we use two-level Bidirectional LSTMs. At each time-step, we obtain a joint embedding by element-wise multiplication of: the *text* embedding (256-d output of the LSTM) and the *image* embedding (2048-d ResNet-50 [17] feature reduced to 256-d using an FC layer). We classify this joint embedding into 9 labels using an FC layer followed by softmax activation.

## 5.2. Methods for VISUAL-centric attributes

Recent deep-learning segmentation methods have proven to be effective in localizing objects based on their visual cues. We propose using a state of the art method in addition to few pretrained methods for VISUAL attributes.

**Pretrained Models (PTM)** We use pretrained methods to classify three classes typically encountered in popular visual scene datasets. (i) `face`: We use bounding box face detections obtained using the Google Cloud Vision API. (ii) `person`: We use the state-of-the-art segmentation method FCIS [32] to predict pixels of COCO class “person” (iii) `lic_plate`: We use OpenALPR [37] to detect license plates in images.

**FCIS** We retrain all layers of the FCIS model [32] for

our task and dataset. We train it for 30 epochs with learning rate 0.0005 over trainval examples and their horizontally mirrored versions. We fine tune it from the model provided by the authors trained for segmentation on MS-COCO [33]. We obtained best results using default hyper-parameters.

## 5.3. Methods for MULTIMODAL-centric attributes

Recognizing Multimodal attributes (e.g. `driv_lic`, `receipt`) require reasoning over both visual and textual domains. We treat this as a classification problem due to: (i) limited training examples ( $\sim 125$  per multimodal attribute) (ii) large region of these attributes ( $\sim 45\%$  image area), which provides only  $\sim 10\%$  utility even after GT-based redaction (Section 4.2).

**Weakly Supervised Labeling (WSL)** We propose learning a multilabel classifier based on visual-only (**WSL:I**) and visual+text content (**WSL:I+T**). If the class probability of an attribute is beyond a certain threshold, we predict all pixels in the image for the attribute. WSL:I is the same approach used in [38] – a multilabel ResNet-50 [17] classifier. In the case of WSL:I+T, we obtain a multimodal embedding by concatenating visual and text representations. We obtain visual representation (identical to WSL:I) with a ResNet-50 architecture. We obtain text representation by encoding all words in the image. We tried three such variants: (i) *Bag-of-Words (BOW) encoding*: Words in the image are represented as a one-hot vector with vocabulary of size 1,751. (ii) *LSTM encoding*: Identical to SEQ, we encode the word sequence using an LSTM with 128-hidden units. We use output from the last cell as the text representation. (iii) *Conv1D encoding*: We use 1D convolutions to encode the word sequence (typically used for sentence classification tasks [25]) followed by max pooling to obtain a fixed-size text representation. In all three cases, we reduce the text-representation to 512-d using an FC+ReLU layer. We report BOW encoding results for **WSL:I+T** in the rest of the paper since this provided the best results.

**Salient Object Prediction (SAL)** Using WSL:I+T as the base classifier, we use the salient object as an approximation of the attribute’s location. We obtain class-agnostic saliency obtained using DeepLab-v2 ResNet [7, 21].

**Weakly Supervised Iterative Refinement (IR)** For document-like objects, the text regions tend to be densely clustered in images. Hence, after classification using WSL:I+T, we refine the convex hull of the text regions using DenseCRF [30] to “spill into” the document region.

## 6. Experiments and Discussion

In this section, we discuss segmentation performance (Section 6.1) and privacy-vs-utility performance (Section 6.2) of our proposed methods.

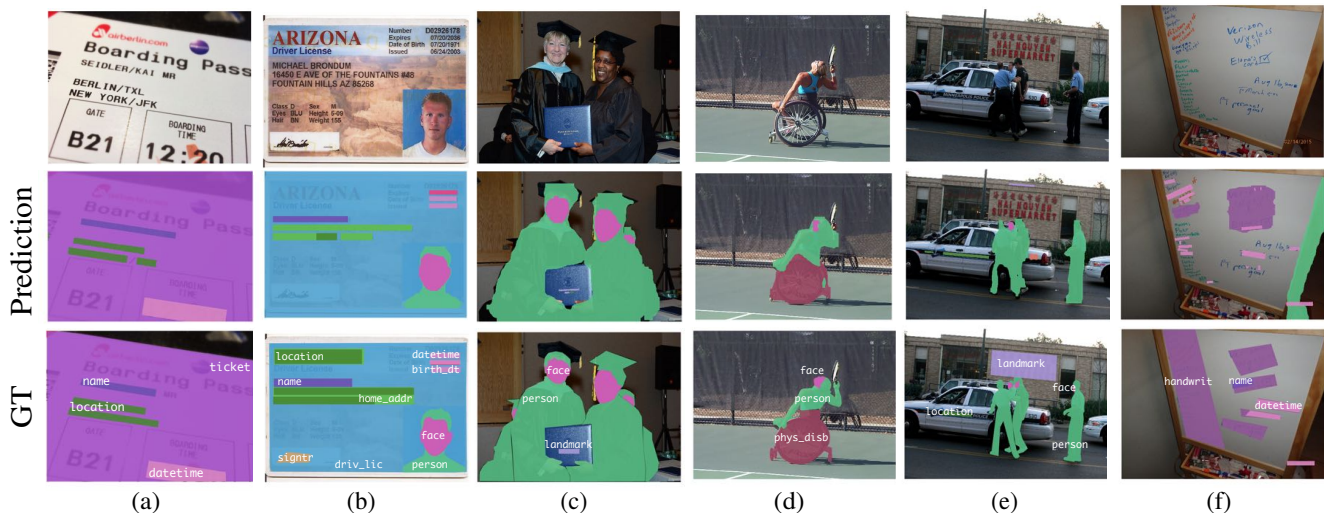


Figure 6: Qualitative examples from our method

## 6.1. Evaluating Segmentation Performance

We now evaluate methods proposed in Section 5 in terms of its segmentation performance using Mean Average Precision, suggested in Pascal VOC [13]. This is calculated by averaging area under precision-recall curves over the privacy attributes. We use 50 thresholds uniformly spaced between 0 and 1 to obtain this curve. At each threshold  $t$ , we: (i) binarize the prediction score masks per image by thresholding pixel-level scores at  $t$  (ii) aggregate pixel-level TP, FP, FN counts (normalized by image size) per attribute over all images to obtain attribute-level precision and recall. We ignore GT masks containing under  $25^2$  pixels during evaluation ( $<1\%$  GT masks).

Table 1 presents the quantitative results of the proposed methods on the test set. Qualitative results in Figure 6 are based on an **ENSEMBLE**, using predictions of SEQ for TEXTUAL, FCIS for VISUAL, WCS:I+T for MULTIMODAL attributes. We generally observe that NN underperforms simple baselines across all modalities, highlighting the difficulty and diversity presented by the dataset.

**TEXTUAL** We observe: (i) *Patterns, frequency and context*: SEQ achieves the best overall score, justifying the need for special methods to tackle text attributes. It is reasonably effective in detecting datetime (Fig. 6a), emailaddr and phone\_no due to patterns they often display. We additionally find SEQ detect attributes which often require prior knowledge (e.g. name, location). The common success modes in such cases are when the words are popular entities (e.g. “Berlin” in Fig. 6a) or have discriminative visual/textual context (e.g. detecting home\_addr in Fig. 6b). (ii) *Challenges imposed by text detections*: PROXY represents an upper bound to our textual methods. The low scores highlights the difficulty of text detection and this is espe-

cially severe for scene and handwritten text detection, a frequent case in our dataset (e.g. Fig. 6e,f). Moreover, our text detections do not perfectly overlap with ground-truth annotations. Since text regions are small, we additionally pay a high performance penalty even for correct detections (e.g. IoU=0.42 for home\_addr in Fig. 6b). Moreover, even in the case of correct text detections, we observe failures in OCR which affects the quality of input for dependent methods. This can be observed by the under-performance of NER, which is typically very effective on clean sanitized text.

**VISUAL** We observe: (i) *The unreasonable effectiveness of FCIS*: We obtain the highest score in the VISUAL category using FCIS. We find FCIS to be highly effective localizing visual objects commonly encountered in other datasets (e.g. person, face). Moreover, we find it achieves reasonable performance even when there is a lack of training data (e.g. only  $<60$  examples of fingerpr, phys\_disb, see Fig. 6d). The common failure modes are either difficult examples (e.g. face in Fig. 6e) or uncommon visual objects (e.g. signtr in Fig. 6b). (ii) *Comparison with Baselines*: PTM achieves comparable results for person, due to Flickr images used to train both models. However, it underperforms for face (detections are not precise enough) and lic\_plate (poor performance in the wild).

**MULTIMODAL** We observe: (i) *WSL:I is a good simple baseline*: WSL:I achieves reasonable performance (45.4) for multimodal attributes, compared to other modes (1.5 in text and 20.8 in visual) although the prediction spans the entire image. This is attributed to large size of MULTIMODAL instances found in images. (ii) *Multimodal reasoning helps*: We find WSL:I+T improves performance over WCS:I by 20%, justifying the need for methods to perform

TEXTUAL										
Method	mAP	location	home addr	name	birth dt	phone no	land mark	date time	email add	
PROXY	45.0	31.7	37.8	48.7	52.5	52.6	33.6	52.4	50.8	
NN	0.5	0.2	0.4	0.1	0.6	0.0	2.0	0.5	0.0	
NER	3.0	6.0	1.7	4.4	0.5	0.0	0.5	10.9	0.0	
RULES	4.2	3.1	0.5	2.8	0.6	1.4	1.2	6.4	17.5	
FCIS	7.2	4.3	0.2	9.8	0.1	2.5	<b>27.6</b>	12.9	0.0	
SEQ	<b>26.8</b>	<b>18.4</b>	<b>19.4</b>	<b>19.1</b>	<b>25.1</b>	<b>45.8</b>	13.9	<b>33.4</b>	<b>38.9</b>	

VISUAL										
Method	mAP	face	license plate	person	nudity	hand writ	physic disb	med hist	fing erpr	signature
NN	13.5	8.4	11.4	33.1	6.0	32.1	11.4	7.4	11.7	0.1
WSL:I+T	20.8	5.0	4.3	30.3	16.4	49.9	13.7	37.7	28.8	1.3
PTM	16.4	47.6	11.6	<b>88.3</b>	0.0	0.0	0.0	0.0	0.0	0.0
FCIS	<b>68.3</b>	<b>83.8</b>	<b>77.9</b>	87.0	<b>69.7</b>	<b>80.7</b>	<b>59.0</b>	<b>45.8</b>	<b>68.1</b>	<b>42.6</b>

MULTIMODAL										
Method	mAP	credit card	passport	driving lic	stud id	mail	receipt	ticket		
NN	21.5	9.8	44.2	17.9	13.0	15.7	16.8	33.3		
WSL:I+T	56.2	29.7	67.4	<b>82.4</b>	<b>58.4</b>	<b>43.3</b>	54.5	57.8		
SAL	36.2	<b>55.9</b>	37.2	23.8	30.4	8.1	42.5	55.1		
IR	53.6	41.7	51.2	67.8	48.1	36.9	57.2	72.5		
FCIS	<b>59.2</b>	53.2	<b>76.3</b>	66.5	50.3	33.1	<b>59.4</b>	<b>75.4</b>		

Table 1: Quantitative results of our methods for segmenting privacy regions. **Bold** numbers denote highest and *italicized* numbers second highest scores in the columns.

multimodal reasoning to detect these attributes. This is particularly necessary to disambiguate similar looking visual objects (e.g. card-like objects `driv.lic` and `stud.id`, Fig. 6b). (iii) *Precision-Recall trade-off*: We find precision for WSL:I+T for this method can be improved for some attributes (e.g. `cr_card`, `ticket`) by IR, which instead of the entire image, predicts only the smoothed hull of text regions. We observe FCIS achieve the best overall score due to higher precision.

## 6.2. Privacy vs. Utility Trade-off by Automatic Redaction

In the previous section, we evaluated our approaches w.r.t. segmentation quality. Now, we ask how effective are redactions based on our proposed methods in terms of privacy and utility?

To answer this, we once again run the user study in Section 4.2 on AMT, but now by redacting proposed pixels of our automated method over those exact images. To vary the number of predicted pixels, we vary the threshold to binarize the predicted score masks over attributes. As a result, we obtain 6-8 redacted versions for each of the 144 images (24 attributes  $\times$  6 images). Each image is labeled by 5 unique qualified AMT workers.

**Results** We obtain privacy-utility scores for each threshold and plot it as a curve in Figure 7. We also plot the

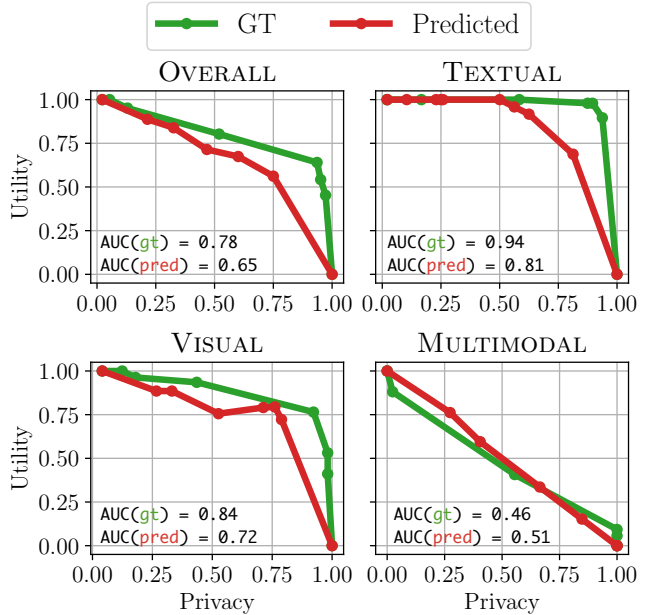


Figure 7: Comparing redactions using predicted and ground-truth segmentations

scores obtained for different dilations of redacted ground-truth annotated region. It should be noted that perfect redactions are unavailable to us and we use these ground-truth based redactions (or manual redactions) only to serve as a reference. We evaluate performance by calculating area under the curve (AUC). We observe: (i) Overall, we find our method obtain a privacy-utility score of 65% – a relative performance of 83% compared to redactions using ground-truth annotation from the dataset. (ii) MULTIMODAL attributes present a hard choice between privacy and utility, as these regions are often large. We find the slightly lower AUC(gt) to be an artifact of sampling. (iii) Although we obtain a low mAP for TEXTUAL attributes, we observe an 81% privacy-utility score. This occurs as we can now over-predict regions, exhibiting low precision and high recall w.r.t. segmentation, but yet retaining high utility due to their small size. Consequently, we can predict more text pixels “for free”.

Based on these observations, we find the automatic redactions of our models trained on the proposed dataset show highly promising results – they closely mimic performance achieved by redacting ground-truth regions across a broad range of private information.

## 7. Conclusion

We proposed a redaction by segmentation approach to aid users selectively sanitize images of private content. To learn automated approaches for this task, we proposed the first sizable visual redactions dataset containing images with pixel-level annotations of 24 privacy attributes. By



conducting a user study, we showed that redacting ground-truth regions in this dataset provides near-perfect privacy while preserving the image’s utility. We then presented automated approaches to segment privacy attributes in images and observed that we can already reasonably segment these attributes. By performing a privacy-vs-utility evaluation of our automated approach, we achieved a highly encouraging 83% performance w.r.t. GT-based redactions.

**Acknowledgement** This research was partially supported by the German Research Foundation (DFG CRC 1223). We thank Anna Khoreva and Alina Dima for feedback on the paper.

## References

- [1] R. Achanta, A. Shaji, K. Smith, A. Lucchi, P. Fua, and S. Süsstrunk. Slic superpixels compared to state-of-the-art superpixel methods. *TPAMI*, 2012. 12
- [2] A. Acquisti and R. Gross. Imagined communities: Awareness, information sharing, and privacy on the facebook. In *PET*, 2006. 2
- [3] C. Bauckhage, A. Jahanbekam, and C. Thurau. Age recognition in the wild. In *ICPR*, 2010. 2
- [4] K. Brkic, I. Sikiric, T. Hrkac, and Z. Kalafatic. I know that person: Generative full body and face de-identification of people in images. In *CVPRW*, 2017. 1, 2, 4
- [5] V. T. Chakaravarthy, H. Gupta, P. Roy, and M. K. Mohania. Efficient techniques for document sanitization. In *CIKM*, 2008. 2
- [6] S.-L. Chang, L.-S. Chen, Y.-C. Chung, and S.-W. Chen. Automatic license plate recognition. *IEEE Trans. Intelligent Transportation Systems*, 2004. 2
- [7] L.-C. Chen, G. Papandreou, I. Kokkinos, K. Murphy, and A. L. Yuille. Semantic image segmentation with deep convolutional nets and fully connected crfs. In *ICLR*, 2015. 6
- [8] R. Chow, P. Golle, and J. Staddon. Detecting privacy leaks using corpus-based association rules. In *KDD*, 2008. 2
- [9] R. Chow, I. Oberst, and J. Staddon. Sanitization’s slippery slope: the design and study of a text revision assistant. In *SOUPS*, 2009. 2
- [10] M. Cordts, M. Omran, S. Ramos, T. Rehfeld, M. Enzweiler, R. Benenson, U. Franke, S. Roth, and B. Schiele. The cityscapes dataset for semantic urban scene understanding. In *CVPR*, 2016. 2, 3
- [11] B. Debatin, J. P. Lovejoy, A.-K. Horn, and B. N. Hughes. Facebook and online privacy: Attitudes, behaviors, and unintended consequences. *Journal of Computer-Mediated Communication*, 2009. 2
- [12] A. Dutta, A. Gupta, and A. Zissermann. Vgg image annotator (via), 2016. <http://www.robots.ox.ac.uk/~vgg/software/via/> Accessed: 2017-11-08. 3
- [13] M. Everingham, L. Van Gool, C. K. I. Williams, J. Winn, and A. Zisserman. The pascal visual object classes (voc) challenge. *IJCV*, 2010. 2, 3, 7, 11
- [14] J. R. Finkel, T. Grenager, and C. D. Manning. Incorporating non-local information into information extraction systems by gibbs sampling. In *ACL*, 2005. 6
- [15] I. Goodfellow, J. Shlens, and C. Szegedy. Explaining and harnessing adversarial examples. In *ICLR*, 2015. 2
- [16] E. T. Hassan, R. Hasan, P. Shaffer, D. Crandall, and A. Kapadia. Cartooning for enhanced privacy in lifelogging and streaming videos. In *CVPRW*, 2017. 1, 4
- [17] K. He, X. Zhang, S. Ren, and J. Sun. Deep residual learning for image recognition. In *CVPR*, 2016. 6
- [18] J. Hendrik Metzen, M. Chaithanya Kumar, T. Brox, and V. Fischer. Universal adversarial perturbations against semantic image segmentation. In *ICCV*, 2017. 2
- [19] Z. Huang, W. Xu, and K. Yu. Bidirectional lstm-crf models for sequence tagging. *arXiv preprint arXiv:1508.01991*, 2015. 6
- [20] S. Joon Oh, R. Benenson, M. Fritz, and B. Schiele. Faceless person recognition; privacy implications in social media. In *ECCV*, 2016. 1
- [21] S. Joon Oh, R. Benenson, A. Khoreva, Z. Akata, M. Fritz, and B. Schiele. Exploiting saliency for object segmentation from image level labels. In *CVPR*, 2017. 6
- [22] S. Joon Oh, M. Fritz, and B. Schiele. Adversarial image perturbation for privacy protection – a game theory perspective. In *ICCV*, 2017. 1, 2
- [23] A. Kae, K. Sohn, H. Lee, and E. Learned-Miller. Augmenting CRFs with Boltzmann machine shape priors for image labeling. In *CVPR*, 2013. 4
- [24] K. Khan, M. Mauro, and R. Leonardi. Multi-class semantic segmentation of faces. In *ICIP*, 2015. 4
- [25] Y. Kim. Convolutional neural networks for sentence classification. In *EMNLP*, 2014. 6
- [26] M. Koestinger, P. Wohlhart, P. M. Roth, and H. Bischof. Annotated facial landmarks in the wild: A large-scale, real-world database for facial landmark localization. In *ICCVW*, 2011. 14
- [27] P. Korshunov, C. Araitho, F. D. Simone, C. Velardo, J.-L. Dugelay, and T. Ebrahimi. Subjective study of privacy filters in video surveillance. *MMSp*, 2012. 2
- [28] P. Korshunov and T. Ebrahimi. Pavid: privacy evaluation video dataset. In *SPIE*, 2013. 2
- [29] P. Korshunov and T. Ebrahimi. Using warping for privacy protection in video surveillance. *DSP*, 2013. 2
- [30] P. Krähenbühl and V. Koltun. Efficient inference in fully connected crfs with gaussian edge potentials. In *NIPS*, 2011. 6
- [31] G. Lample, M. Ballesteros, S. Subramanian, K. Kawakami, and C. Dyer. Neural architectures for named entity recognition. In *NAACL*, 2016. 6
- [32] Y. Li, H. Qi, J. Dai, X. Ji, and Y. Wei. Fully convolutional instance-aware semantic segmentation. In *CVPR*, 2017. 2, 6
- [33] T.-Y. Lin, M. Maire, S. Belongie, J. Hays, P. Perona, D. Ramanan, P. Dollár, and C. L. Zitnick. Microsoft coco: Common objects in context. In *ECCV*, 2014. 2, 3, 6, 11
- [34] J. Long, E. Shelhamer, and T. Darrell. Fully convolutional networks for semantic segmentation. In *CVPR*, 2015. 2

- [35] X. Ma and E. Hovy. End-to-end sequence labeling via bi-directional lstm-cnns-crf. In *ACL*, 2016. 6
- [36] S.-M. Moosavi-Dezfooli, A. Fawzi, O. Fawzi, and P. Frossard. Universal adversarial perturbations. In *CVPR*, 2017. 2
- [37] Openalpr. <https://github.com/openalpr/openalpr>. Accessed: 2017-11-08. 6
- [38] T. Orekondy, B. Schiele, and M. Fritz. Towards a visual privacy advisor: Understanding and predicting privacy risks in images. In *ICCV*, 2017. 1, 2, 6
- [39] J. Pennington, R. Socher, and C. D. Manning. Glove: Global vectors for word representation. In *EMNLP*, 2014. 6
- [40] N. Raval, A. Machanavajjhala, and L. P. Cox. Protecting visual secrets using adversarial nets. In *CVPRW*, 2017. 1
- [41] D. Sánchez and M. Batet. Toward sensitive document release with privacy guarantees. *Engineering Applications of AI*, 2017. 2
- [42] D. Sánchez, M. Batet, and A. Viejo. Detecting sensitive information from textual documents: An information-theoretic approach. In *MDAI*, 2012. 2
- [43] D. Sánchez, M. Batet, and A. Viejo. Automatic general-purpose sanitization of textual documents. *IEEE Transactions on Information Forensics and Security*, 2013. 2
- [44] M. Shao, L. Li, and Y. Fu. What do you do? occupation recognition in a photo via social context. In *ICCV*, 2013. 2
- [45] M. Sharif, S. Bhagavatula, L. Bauer, and M. K. Reiter. Accessorize to a crime: Real and stealthy attacks on state-of-the-art face recognition. In *ACM CCS*, 2016. 2
- [46] Q. Sun, B. Schiele, and M. Fritz. A domain based approach to social relation recognition. In *CVPR*, 2017. 2
- [47] X. Sun, P. Wu, and S. C. H. Hoi. Face detection using deep learning: An improved faster rcnn approach. *CoRR*, 2017. 2
- [48] A. Tonge and C. Caragea. Privacy prediction of images shared on social media sites using deep features. *arXiv preprint arXiv:1510.08583*, 2015. 2
- [49] P. A. Viola and M. J. Jones. Robust real-time face detection. *IJCV*, 2001. 2
- [50] G. Wang, A. C. Gallagher, J. Luo, and D. A. Forsyth. Seeing people in social context: Recognizing people and social relationships. In *ECCV*, 2010. 2
- [51] E. S. Xioufis, S. Papadopoulos, A. Popescu, and Y. Kompatsiaris. Personalized privacy-aware image classification. In *ICMR*, 2016. 2
- [52] S. Zerr, S. Siersdorfer, J. Hare, and E. Demidova. I know what you did last summer!: Privacy-aware image classification and search. In *ACM SIGIR*, 2012. 2
- [53] H. Zhang, W. Jia, X. He, and Q. Wu. Learning-based license plate detection using global and local features. In *International Conference on Pattern Recognition (ICPR)*, 2006. 2
- [54] W. Zhou, H. Li, Y. Lu, and Q. Tian. Principal visual word discovery for automatic license plate detection. *IEEE Transactions on Image Processing*, 2012. 2

# Appendices

## A. Contents

The appendix contains:

- Detailed descriptions, examples and auxiliary analysis of the 24 privacy attributes discussed in Section 3.2
- Precision-Recall curves for the methods discussed in Table 1
- Qualitative results to supplement Figure 6
- Implementation details and qualitative results to supplement Section 4 and Section 6.2

## B. Privacy Attributes

In this section, we provide detailed descriptions and examples of the 24 Privacy Attributes used in the proposed dataset. We also present a brief supplementary analysis of the conditional co-occurrence of these attributes in the dataset.

**Detailed Descriptions and Instructions** In Figures 10-12, we provide detailed descriptions and examples of the 24 privacy attributes grouped by category, which was discussed in Section 3.2. The descriptions briefly summarize the instructions provided to the annotators. The figures displays instance-agnostic ground-truth annotations of respective attributes. Ground-truth annotations are stored in a format similar to MS-COCO [33].

TEXTUAL, signtr and handwrit attributes are annotated using 4-sided polygons or bounding-boxes. For TEXTUAL attributes, only Latin-based words understandable by English-speakers are annotated. For remaining attributes, the objects are enclosed in a polygon. In case of severe occlusion, the object is enclosed using multiple polygons.

**Auxiliary Privacy Attribute Analysis** Figure 8 represents the conditional co-occurrence matrix (*i.e.* probability that attribute  $X$  occurs in an image containing attribute  $Y$ ) of the 24 privacy attributes in images. The privacy attributes along rows and columns are sorted by category. From this plot, we find: (i) Images of MULTIMODAL attributes often appear alongside a variety of TEXTUAL attributes (bottom-left block of matrix). (ii) However, the contrary is not true – TEXTUAL attributes do not frequently occur only in the presence of MULTIMODAL attributes (top-right block of matrix). (iii) person and face occur frequently alongside other VISUAL attributes as they are central to many common visual scenes (central block of matrix).

## C. Precision Recall Curves

The Precision-Recall curves of methods proposed in Table 1 are presented in Figure 9. The first column represents averaged category performance. We plot these curves

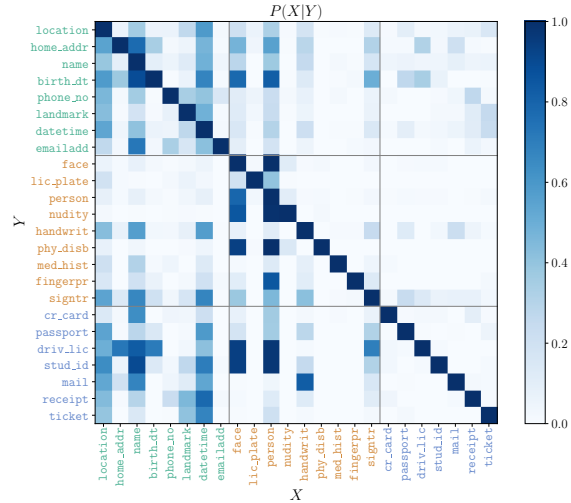


Figure 8: Conditional co-occurrence matrix. Groups of attributes are sorted by categories. Color codes used for attribute categories: TEXTUAL, VISUAL, MULTIMODAL

by thresholding our methods at 50 uniform intervals in the range  $[0, 1]$ . Similar to Pascal VOC [13], we correct the curves to have monotonically decreasing precision by setting precision at  $r$  to be the highest precision at  $r' \geq r$ . Moreover, precision at  $r = 0$  is extrapolated as highest precision at  $r' \geq 0$ . We calculate Average Precision as area under this curve using trapezoidal rule.

**Auxiliary Discussion** From PR curves in Figure 9, we observe: (i) The under-performance NN indicates diversity and difficulty of the dataset. (ii) TEXTUAL: We find the best performance using SEQ. PROXY denotes a rough upper bound. We find SEQ obtain slightly higher recall as it predicts overlapping masks. (iii) VISUAL: We find FCIS achieve the best performance. For person, we find a similar curve with PTM since both have the same architecture and images from the same domain (Flickr) used for training. (iv) MULTIMODAL: FCIS achieves slightly higher category performance compared to others. WCS:I+T generally achieves better recall across all attributes. IR/SAL improves precision of WCS:I+T by trading off recall.

## D. Qualitative Results for Segmentation

We present qualitative results in Figure 16 to supplement results in Figure 6 and discussion in Section 6.1. We present the qualitative results per attribute, sorted by their Intersection Over Union (IoU) Scores. Hence, figures on top represent common success modes and figures at the bottom represent common failure modes. These results were obtained using ENSEMBLE by choosing the operating point with the highest IoU score per mode.

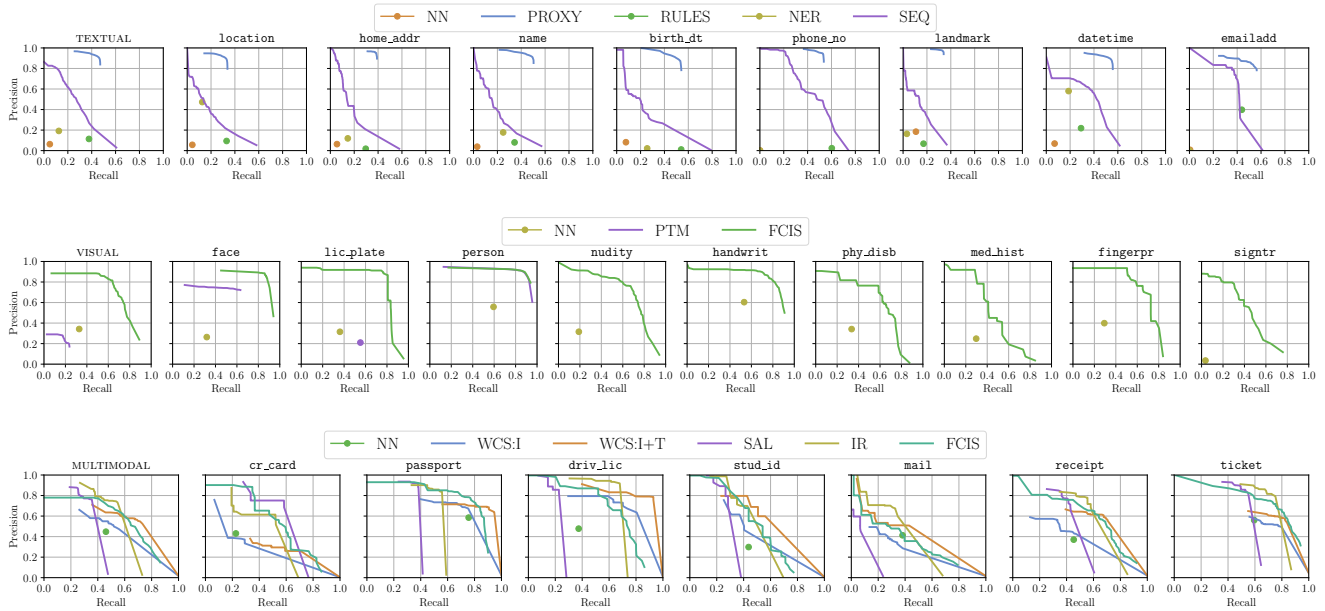


Figure 9: Precision-Recall curves for methods in Table 1

## E. Privacy vs. Utility Trade-off

In this section, we provide implementation details on the redaction scaling strategy used for ground-truth redactions (Section 4.1) and predicted redactions (Section 6.1). In both cases, we perform a black-out of relevant pixels. For `phy_disb`, we black-out w.r.t. a bounding-box region since we observed the silhouette is a strong visual indicator of the attribute. In addition, we provide qualitative results for these strategies in Figures 17 and 18 to supplement Figure 3.

**Scaling Ground-truth Redactions** We scale ground-truth redactions using super-pixels to roughly adhere to edges and object boundaries. The downscaled image is first represented using 3000-5000 superpixels generated using SLIC0 [1]. We represent the ground-truth binary mask per attribute using a 0-1 labeling over the graph of superpixels, where 1 represents the node (superpixel) belongs in the redaction. To *dilate*, we iteratively add 0-nodes with most number of adjacent 1-nodes. To *erode*, we perform the same operation with an inverted ground-truth binary-mask. We parameterize the scaling using  $s \in S$  (where  $S = \{0.0, 0.25, 0.5, 1.0, 2.0, 4.0, \text{inf}\}$ ), representing the dilation/erosion factor of the ground-truth mask.

**Scaling Predicted Redactions** From the ENSEMBLE method, we obtain softmax probability score masks  $\mathbb{R}^{w \times h \times k}$  for  $k$  attributes per image. We compute multiple thresholds per attribute to binarize the score masks, such that at threshold  $t \in T$ ,  $t$  times the number of ground-truth

attribute pixels are redacted over the entire test-set of images. We use  $T = \{0.25, 0.5, 1.0, 2.0, 4.0, 8.0\}$ . For TEXTUAL attributes, we use an additional threshold such that all detected text is redacted.

**Qualitative Results Auxiliary Discussion** Figure 17 and 18 displays examples of common success and failure modes w.r.t. to the attribute mentioned. All images in these figures are from the test set.  $P$  and  $U$  indicate privacy and utility score, which is simply the percentage of  $\sim 5$  AMT workers who agree to the privacy and utility questions. High  $P$  indicates the image is private w.r.t. to attribute  $a$  and high  $U$  indicates the image is intelligible. In these figures, we find: (i) For small private regions, we can redact more pixels without affecting utility (Figure 17 `location` and `face`) (ii) MULTIMODAL attributes often display a hard choice between privacy and utility (Figure 17 `mail`) (iii) Text detections or OCR is a common failure mode with handwritten text for automatic redactions (Figure 18 `home_addr`) (iv) Some difficult MULTIMODAL attributes (Figure 18 `stud_id`) can be detected only at high thresholds, entailing complete redactions of many FP images too (v) Figure 18 `fingerpr` represents one of the failure cases for ground-truth redaction discussed in Section 4.3, where AMT turkers overlook details in the question. In this particular case, the workers were asked to only consider fingerprints from fingertips. However, even at  $s = 1$  where the finger-tips are redacted, many workers incorrectly answer fingerprints as being visible.


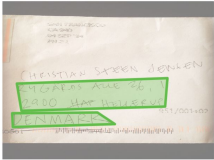


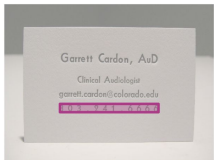



Attribute	Example	Description
Location (location)		Region of the image depicting where the photographer might have visited. Includes the following cases: Street signs, addresses, GPS co-ordinates, flags.
Home Address (home_addr)		Someone's home address based on the context, such as on an identity card or mail.
Name (name)		Someone's name such as on a name-tag or identity card. Any recognizable name in Latin-based text is included, including that of popular figures.
Birth Date (birth_dt)		Someone's date of birth (day, month and/or year) determined based on context, such as on identity cards or passports.
Phone no. (phone_no)		A syntactically-correct phone number (either personal or business), determined either based on context or pattern.
Landmark (landmark)		Name of a store, restaurant or a business such as on a store front or a receipt.
Date/Time (datetime)		A date or time, such as revealing a time-frame when the photograph might have been captured.
Email address (emailadd)		A syntactically-correct email address

Figure 10: Descriptions and examples of TEXTUAL attributes. privacy attributes. For readability, we display images where attributes are salient.




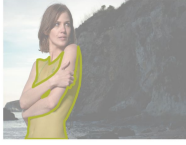





Attribute	Example	Description
Face (face)		Region indicating a person's face, containing all visible facial landmarks discussed in [26]. Regions occluded by hair or masks are excluded.
License Plate (lic_plate)		Region containing a license plate or vehicle registration or identification number in any language/country. We consider any motorized vehicle (e.g. cars, motorbike, train).
Person (person)		Region indicating any part of a person or their reflections. Includes person's body along with wearables (e.g. hats, goggles, backpacks). Excludes objects the person is holding (e.g. shopping bag, guitar).
Nudity (nudity)		Torso and thigh region of a person, if skin is completely/partially visible in this region.
Handwriting (handwrit)		Someone's handwritten text in any language.
Physical Disability (phy_disb)		Region indicating either a) special equipment used by a physically disabled person (e.g. wheelchair) or b) region around limbs, if limbs are absent.
Medical History (med_hist)		Any pharmaceutical consumable such as pills, capsules or syrups (including their containers and packaging).
Fingerprint (fingerpr)		Someone's finger-tips if ridges are clearly visible upon zooming-in or fingerprint impressions on any surface.
Signature (signtr)		Region indicating someone's signature

Figure 11: Descriptions and examples of VISUAL attributes. For readability, we display images where attributes are salient.







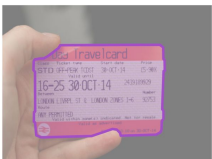
Attribute	Example	Description
Credit Card (cr_card)		Either front, rear or any details of a credit card or similar monetary instrument
Passport (passport)		Any page (including cover) of a Passport
Drivers License (driv_lic)		Front, rear or written details of a Drivers License or driving permit
Student ID (stud_id)		Front or rear of a student identity card
Mail (mail)		Mail including hand-written letters, post-cards or packages
Receipt (receipt)		A document indicating a financial transaction, such as receipts or checks
Ticket (ticket)		A ticket, such as for travel, concert or sports match

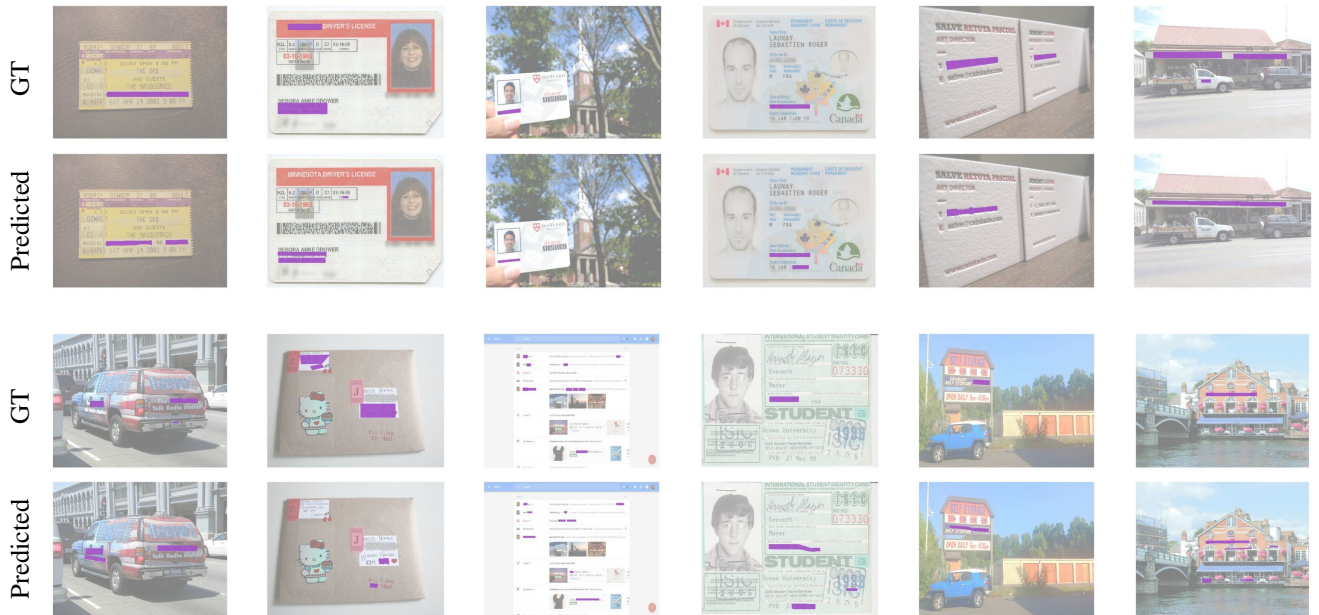
Figure 12: Descriptions and examples of MULTIMODAL attributes. For readability, we display images where attributes are salient.

location      home\_addr      name      birth\_dt      phone\_no      landmark

good (iou ≥ 0.75)



mediocre (0.25 ≤ iou < 0.75)



failure (iou ≈ 0)



Figure 13: Qualitative results per attribute. In each pair of images, top is ground-truth segmentation and bottom is prediction. Pairs of images in each column are sorted by IoU scores (high to low).



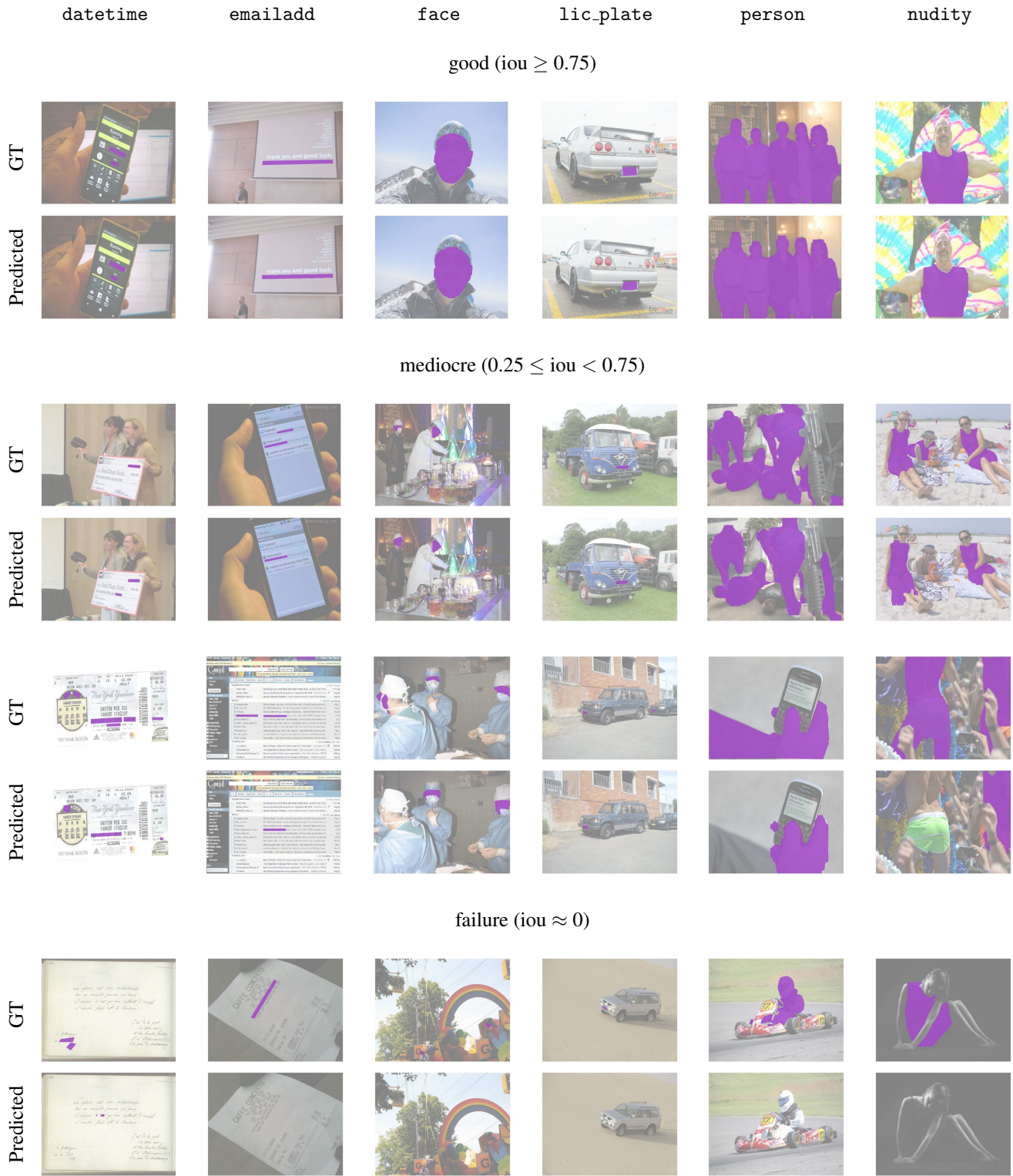


Figure 14: Qualitative results per attribute. In each pair of images, top is ground-truth segmentation and bottom is prediction. Pairs of images in each column are sorted by IoU scores (high to low).

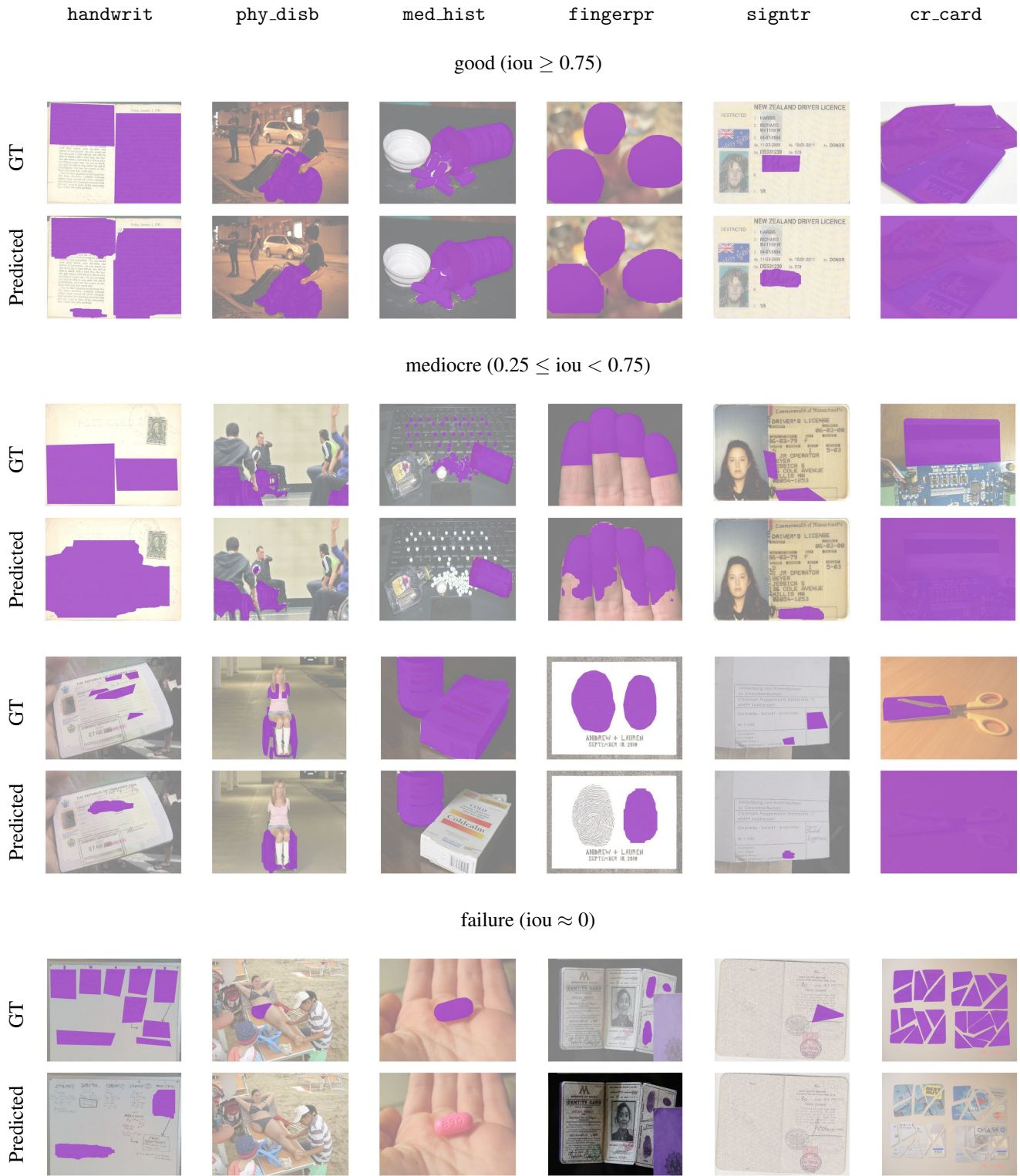


Figure 15: Qualitative results per attribute. In each pair of images, top is ground-truth segmentation and bottom is prediction. Pairs of images in each column are sorted by IoU scores (high to low).

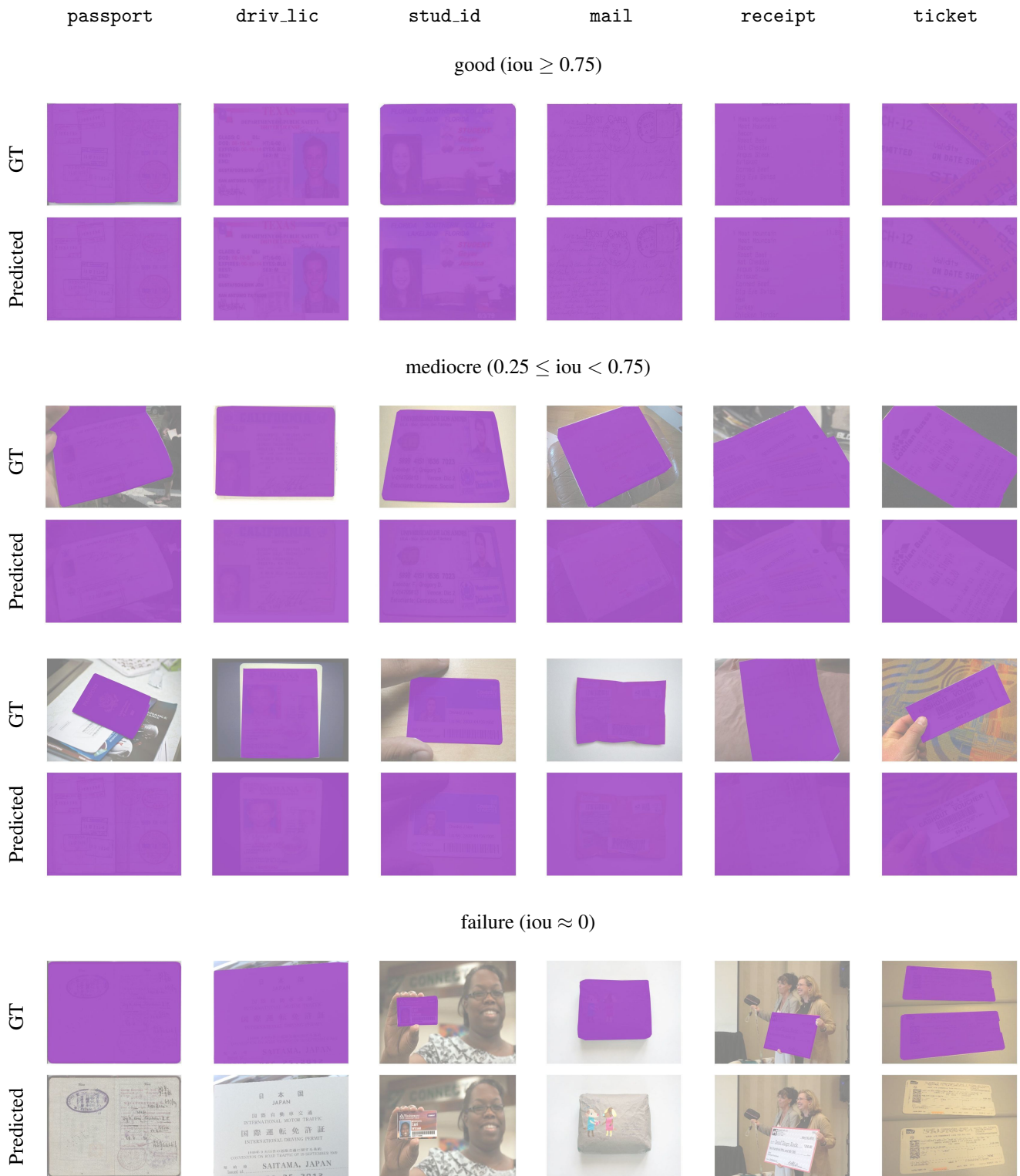


Figure 16: Qualitative results per attribute. In each pair of images, top is ground-truth segmentation and bottom is prediction. Pairs of images in each column are sorted by IoU scores (high to low).

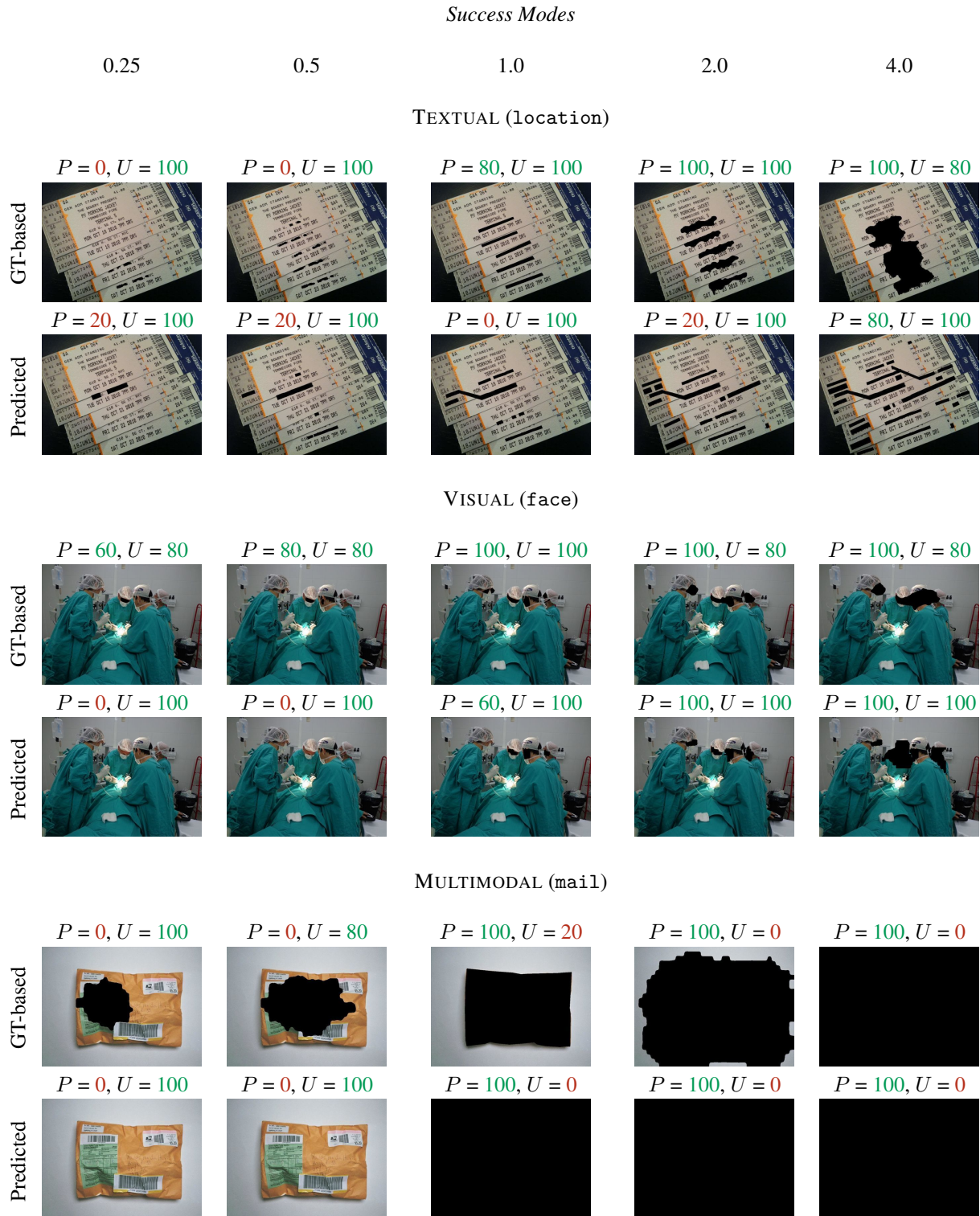


Figure 17: *Common Success Modes of Automatic Redactions*. GT-based are ground-truth regions scaled and redacted as discussed previously. Predicted are automatic redactions generated by method ENSEMBLE.  $P$  indicates privacy score and  $U$  indicates utility score. In both cases, higher is better. Scores are indicated in green in case of majority agreement and red otherwise.

### Failure Modes

0.25

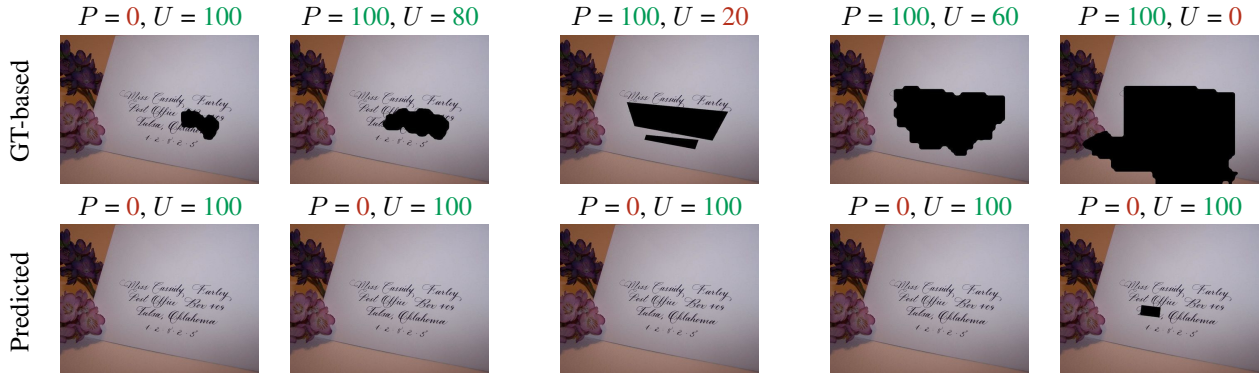
0.5

1.0

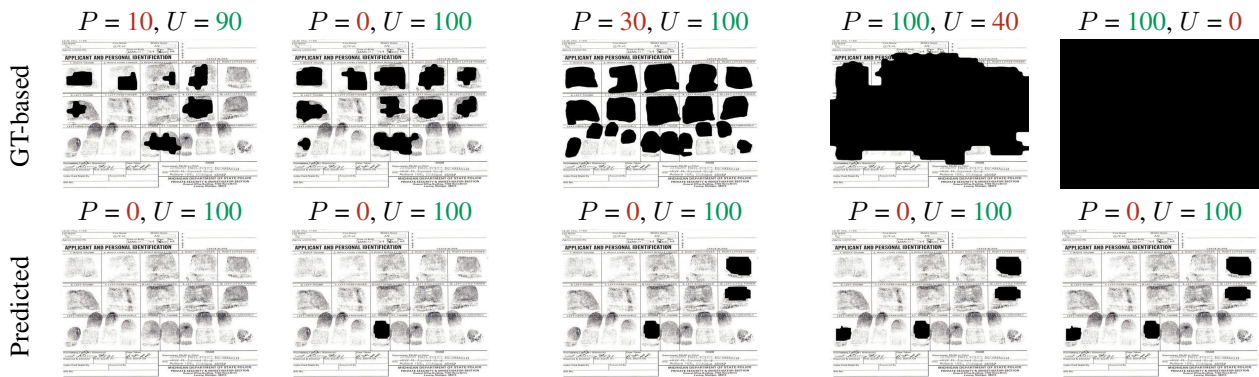
2.0

4.0

#### TEXTUAL (home\_addr)



#### VISUAL (fingerpr)



#### MULTIMODAL (stud\_id)

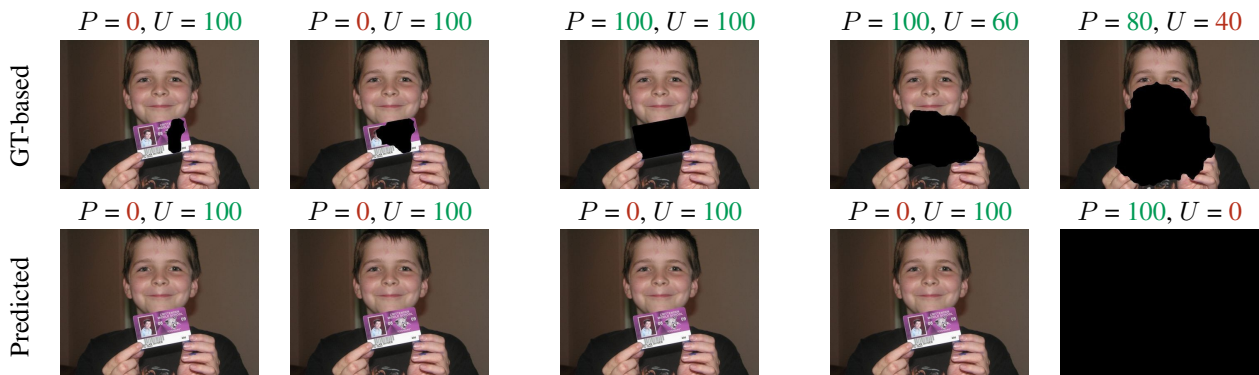


Figure 18: *Common Failure Modes of Automatic Redactions*. GT-based are ground-truth regions scaled and redacted as discussed previously. Predicted are automatic redactions generated by method ENSEMBLE.  $P$  indicates privacy score and  $U$  indicates utility score. In both cases, higher is better. Scores are indicated in green in case of majority agreement and red otherwise.